



Cite this: *Nanoscale Adv.*, 2025, 7, 3456

Received 27th January 2025  
Accepted 9th April 2025

DOI: 10.1039/d5na00096c

rsc.li/nanoscale-advances

## Raman spectroscopy of 2D MoS<sub>2</sub> on Ti<sub>3</sub>C<sub>2</sub> MXene: the substrate effect†

Ethan Pollack, Qiaohui Zhou, Elham Loni, Kenneth Agbakansi, Ahmad Majed, Fei Wang, Ali Soleymani, Melena Busse, Michael Naguib and Xin Lu \*

We use Raman spectroscopy to study the substrate effect of Ti<sub>3</sub>C<sub>2</sub> MXene on the lattice vibrational modes of MoS<sub>2</sub>. We observed redshifts in the fingerprint peaks of MoS<sub>2</sub>, and explained the shifts based on their vibrational nature. The shift in the in-plane E<sub>2g</sub><sup>1</sup> mode is attributed to the strain effect, and the softened A<sub>1g</sub> mode associated with the out-of-plane vibration is caused by electron doping. In addition to monolayer MoS<sub>2</sub>, we show that the modulation from Ti<sub>3</sub>C<sub>2</sub> MXene is also present in few-layer and bulk MoS<sub>2</sub>. Furthermore, we demonstrate that the laser-induced shift occurs even at low excitation power. Our results indicate that a detailed power-dependent measurement is indispensable for extracting the pure substrate effect from Raman spectroscopy.

### Introduction

MXenes refer to a group of two-dimensional (2D) transition metal carbides, carbonitrides, and nitrides. With the chemical formula of M<sub>n+1</sub>X<sub>n</sub>T<sub>x</sub> (M is a transition metal; X is carbon/nitrogen/oxygen; T denotes surface terminations), the family of MXene includes a variety of compositions and diverse properties,<sup>1</sup> and hence holds great promise in energy storage,<sup>2</sup> catalysis,<sup>3</sup> electronics,<sup>4</sup> and sensing.<sup>5,6</sup> In recent years, the stacking of MXenes with other 2D materials, such as semiconducting transition metal dichalcogenides (TMDs), has attracted growing interest in nanoelectronics<sup>7</sup> and catalysis. For instance, spray-coated Ti<sub>3</sub>C<sub>2</sub> MXene films can work as metal contacts and be integrated into MoS<sub>2</sub> transistor circuits for large-scale 2D electronics.<sup>8</sup> Due to the larger interlayer spacing, vertically aligned MoS<sub>2</sub> on Ti<sub>3</sub>C<sub>2</sub> has been shown to be an improved catalyst in the hydrogen evolution reaction.<sup>9</sup> Similarly, in tribology, the hybrid Ti<sub>3</sub>C<sub>2</sub>-MoS<sub>2</sub> coatings result in super-lubricious behavior and demonstrate even better lubricity performance than MoS<sub>2</sub>.<sup>10</sup> Despite the various applications of such hybrids, a detailed study on the interfacial interaction between Ti<sub>3</sub>C<sub>2</sub> MXene and MoS<sub>2</sub> is still lacking. In particular, how the presence of the Ti<sub>3</sub>C<sub>2</sub> MXene film affects the lattice vibrations and structure of MoS<sub>2</sub> remains largely unexplored.

With the intensive research on TMDs in the past decade, influence of the environment, including the substrate effect and the modulation from the adjacent material, has been extensively studied *via* optical spectroscopy.<sup>11–16</sup> In this work, we use

Raman spectroscopy as a nondestructive and rapid tool to probe the interfacial interaction between Ti<sub>3</sub>C<sub>2</sub> MXene and MoS<sub>2</sub>. The Ti<sub>3</sub>C<sub>2</sub> MXene flakes were exfoliated from Ti<sub>3</sub>C<sub>2</sub> MXene free-standing paper (see Methods). The monolayer MoS<sub>2</sub> samples were prepared by mechanical exfoliation from a bulk crystal (2D semiconductor). We fabricated the MoS<sub>2</sub>-Ti<sub>3</sub>C<sub>2</sub> stack using the polydimethylsiloxane-based dry-transfer method<sup>17</sup> or the pick-up technique,<sup>18</sup> followed by thermal annealing. Samples prepared using the pick-up technique have a hexagonal boron nitride (h-BN) layer on top for additional protection, but we note that the modulation from Ti<sub>3</sub>C<sub>2</sub> MXene does not depend on the top h-BN layer. Fig. 1a shows a schematic diagram of the as-stacked structure with a monolayer (1L) MoS<sub>2</sub> flake placed on the Ti<sub>3</sub>C<sub>2</sub> MXene multilayer. Another 1L MoS<sub>2</sub> flake is placed on the Si/SiO<sub>2</sub> substrate as a reference. In order to simulate the structures used in electronic and catalytic applications, the Ti<sub>3</sub>C<sub>2</sub> MXene flakes we prepared are thick (Fig. 1b). The 1L MoS<sub>2</sub> (~0.7 nm) appears green/blue on the 285 nm SiO<sub>2</sub> oxide layer (not shown in Fig. 1b), consistent with previous studies,<sup>19,20</sup> but it “disappears” on the Ti<sub>3</sub>C<sub>2</sub> MXene multilayer due to the optical interference effect.<sup>11</sup>

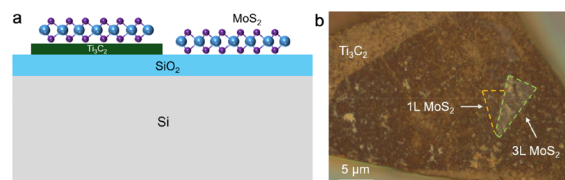


Fig. 1 Fabrication of the MoS<sub>2</sub>-Ti<sub>3</sub>C<sub>2</sub> MXene stack. (a) Schematic illustration of 1L MoS<sub>2</sub> on the Ti<sub>3</sub>C<sub>2</sub> MXene flake and the Si/SiO<sub>2</sub> substrate. (b) An optical image of the MoS<sub>2</sub>-Ti<sub>3</sub>C<sub>2</sub> MXene heterostructure.

Department of Physics and Engineering Physics, Tulane University, New Orleans, Louisiana 70118, USA. E-mail: xlu5@tulane.edu

† Electronic supplementary information (ESI) available. See DOI: <https://doi.org/10.1039/d5na00096c>



## Results and discussion

### Thickness-dependent Raman spectra of MoS<sub>2</sub>

Before discussing the interfacial interaction from Ti<sub>3</sub>C<sub>2</sub> MXene on the lattice vibrational modes in MoS<sub>2</sub>, we first measured the Raman spectra of MoS<sub>2</sub> on the Si/SiO<sub>2</sub> substrate. Fig. 2a demonstrates the non-resonant Raman spectra of 1-4L and bulk MoS<sub>2</sub> by using a 532 nm laser. We focus on the fingerprint peaks, A<sub>1g</sub> and E<sub>2g</sub> modes. The A<sub>1g</sub> peak, which involves the out-of-plane displacements of S atoms in each layer, blue-shifts from ~405 cm<sup>-1</sup> in 1L to ~409 cm<sup>-1</sup> in bulk (Fig. 2a and b). As shown in the atomic displacements (Fig. 2e), when the thickness increases, the adjacent S atoms vibrate out-of-phase. Within the classical model for coupled oscillators, the interlayer van der Waals (vdW) interaction causes larger effective forces in thicker flakes, thus stiffening the A<sub>1g</sub> mode.<sup>21,22</sup> The vdW model, which includes the influence of interlayer coupling on the intralayer vibration,<sup>23</sup> has been introduced to explain the Davydov splitting in bulk and bilayer layered materials.<sup>24,25</sup> We applied the vdW model to the A<sub>1g</sub> mode in 2L MoS<sub>2</sub> by following the equation  $\omega_c^2 = \omega_0^2 + \Delta\omega^2$ , where  $\omega_0$  is the frequency of the two uncoupled oscillators when the two neighboring sulfur atoms vibrate in-phase (A<sub>2u</sub>, Raman-inactive),  $\omega_c$  is the frequency when neighboring sulfur atoms vibrate out-of-phase (A<sub>1g</sub>, Fig. 2e right) and  $\Delta\omega$  is the coupling frequency between the two entities. In the first-order approximation,  $\Delta\omega$  can be considered the energy of the interlayer breathing (LB) mode, whose energy is 40.0 cm<sup>-1</sup> in our 2L MoS<sub>2</sub> (Fig. S1†). With  $\omega_c = 406.3$  cm<sup>-1</sup> and  $\Delta\omega = 40.0$  cm<sup>-1</sup> in 2L, we obtain  $\omega_0 = 404.3$  cm<sup>-1</sup>, which indicates that the Raman-inactive A<sub>2u</sub> mode is red-shifted compared to the A<sub>1g</sub> mode in 1L (with symmetry of A<sub>1</sub> in odd layer numbers). This result is intuitive with the classical model since the equivalent force constant from two springs in series would be smaller than either one of the oscillators.

While the thickness effect explains the shift of the A<sub>1g</sub> mode, due to its in-plane vibrational nature, the E<sub>2g</sub> mode should be less sensitive to the thickness (Fig. 2e left). As a result, one would expect a smaller blue-shift or no-shift of the E<sub>2g</sub> mode with increasing thickness. The anomalous redshift (Fig. 2a and

c) was once thought to originate from the dielectric effect. Nevertheless, the dielectric effect was ruled out by Lin *et al.*<sup>26</sup> They placed exfoliated MoS<sub>2</sub> in different solvents with dielectric constants ranging from 1.89 to 32.6 but observed no systematic Raman shifts. Later, Luo *et al.* attributed the red-shift of the E<sub>2g</sub> mode with increasing thickness to the surface effect, which refers to the larger Mo–S force constants at the surface of atomically thin MoS<sub>2</sub> due to the loss of neighboring adjacent layers.<sup>22</sup> The larger force constant increases the Raman shift of the E<sub>2g</sub> mode in thinner layers, causing the peak to blue-shift.<sup>27–29</sup> The energy difference between the A<sub>1g</sub> and E<sub>2g</sub> modes ( $\text{Pos}(A_{1g}) - \text{Pos}(E_{2g})$ ) has been shown to correlate with the thickness.<sup>21</sup> Our measured results show that the difference is ~19 cm<sup>-1</sup> in 1L MoS<sub>2</sub> and reaches ~25 cm<sup>-1</sup> in bulk MoS<sub>2</sub> (Fig. 2d), which is consistent with earlier results.<sup>21,27–29</sup> The consistency indicates that unintentional strain<sup>30,31</sup> and doping effects<sup>32,33</sup> are absent in our exfoliated samples (compared to samples on Si/SiO<sub>2</sub> only).

### Raman and PL spectra of the 1L MoS<sub>2</sub>-Ti<sub>3</sub>C<sub>2</sub> MXene stack

We plotted the Raman spectra of h-BN capped, 1L MoS<sub>2</sub> on Ti<sub>3</sub>C<sub>2</sub> MXene and on a Si/SiO<sub>2</sub> substrate. As shown in Fig. 3a, the A<sub>1g</sub> and E<sub>2g</sub> modes from 1L MoS<sub>2</sub> on Si/SiO<sub>2</sub> are located at 406.5 cm<sup>-1</sup> and 386.5 cm<sup>-1</sup>, respectively, with the energy difference being 20 cm<sup>-1</sup>. Compared to the Raman shifts in Fig. 2d, the larger energy difference (20 cm<sup>-1</sup> vs. 19 cm<sup>-1</sup>) is mainly due to the blue-shifted A<sub>1g</sub> mode (406.5 cm<sup>-1</sup> vs. ~405 cm<sup>-1</sup>). The stiffened A<sub>1g</sub> mode resembles the thickness effect in few-layer MoS<sub>2</sub>, where the interlayer vdW interaction increases the effective force constant. Here, the thickness effect results from interlayer interaction with the top h-BN layer which also has a hexagonal lattice. Note that both samples (on Ti<sub>3</sub>C<sub>2</sub> MXene and on Si/SiO<sub>2</sub>) are capped with h-BN, so the comparison is still valid.

Compared with MoS<sub>2</sub> on Si/SiO<sub>2</sub>, the A<sub>1g</sub> and E<sub>2g</sub> modes of MoS<sub>2</sub> on Ti<sub>3</sub>C<sub>2</sub> MXene red-shift by 3.3 cm<sup>-1</sup> and 2.9 cm<sup>-1</sup>, respectively. To analyze the shifts, we started by first ruling out other possible factors. Since the redshifts persist after thermal annealing, we do not think adsorption on the surface of MoS<sub>2</sub> plays a major role. Meanwhile, even if the interaction between MoS<sub>2</sub> and Ti<sub>3</sub>C<sub>2</sub> MXene introduces new resonances, the energies of both phonon modes are constant across a wide range of excitation lasers.<sup>34</sup> Therefore, we further ruled out the resonance effect. The charge transfers between Ti<sub>3</sub>C<sub>2</sub> MXene and MoS<sub>2</sub> could result in a doping effect in MoS<sub>2</sub>. However, Chakraborty *et al.* demonstrated that the doping effect has a negligible influence on the E<sub>2g</sub> mode,<sup>32</sup> which does not match with our observed features. As a result, we believe that the possible cause of softened peaks, especially the E<sub>2g</sub> mode, is strain. It is hard to completely get rid of strain in layered materials particularly when there is a lattice mismatch. In addition, the sample preparation process, whether through the pick-up technique or the polydimethylsiloxane-based dry-transfer method, may introduce even larger strain into the flakes. Rather than exhibiting uniaxial strain, when the layered material is stretched or compressed in one specific direction, the strain that MoS<sub>2</sub>

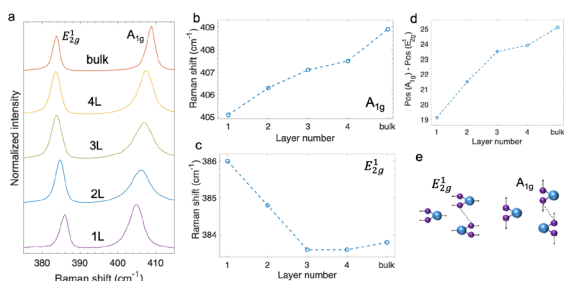


Fig. 2 Layer-dependent Raman spectroscopy of MoS<sub>2</sub> on the Si/SiO<sub>2</sub> substrate. (a) Raman spectra of 1-4L and bulk MoS<sub>2</sub> in the range of 375 cm<sup>-1</sup> to 415 cm<sup>-1</sup>. (b–d) Thickness-dependent shift of the A<sub>1g</sub> mode (b), E<sub>2g</sub> mode (c), and the energy difference of A<sub>1g</sub> and E<sub>2g</sub> modes (d). (e) Displacement representations of A<sub>1g</sub> and E<sub>2g</sub> modes in 1L and 2L MoS<sub>2</sub>.



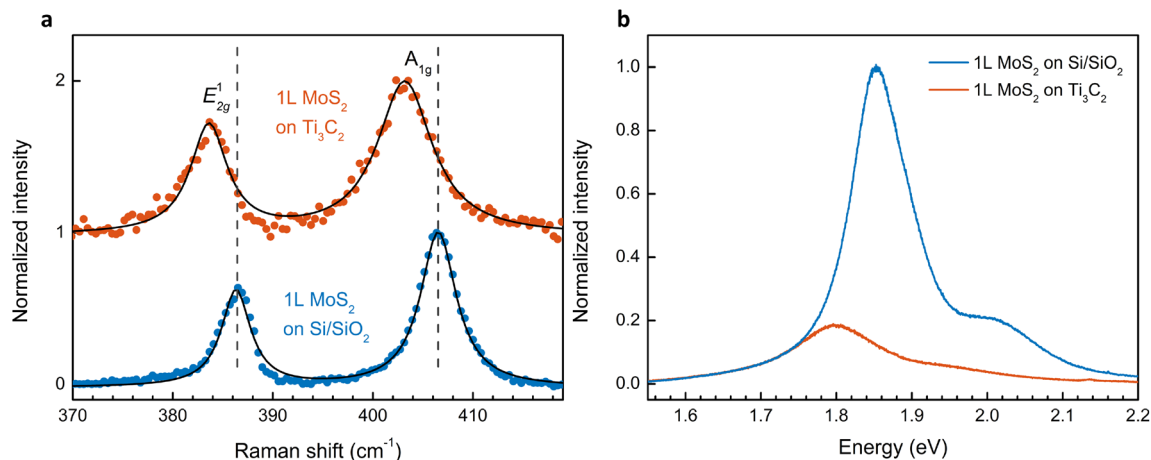


Fig. 3 Comparison of 1L MoS<sub>2</sub> on Ti<sub>3</sub>C<sub>2</sub> MXene and 1L MoS<sub>2</sub> on Si/SiO<sub>2</sub>. (a) Raman spectra of 1L MoS<sub>2</sub> on Ti<sub>3</sub>C<sub>2</sub> MXene and 1L MoS<sub>2</sub> on Si/SiO<sub>2</sub>. Dots represent the experimental data and lines correspond to the Lorentzian fitting. (b) Photoluminescence (PL) spectra of 1L MoS<sub>2</sub> on Ti<sub>3</sub>C<sub>2</sub> MXene in comparison with 1L MoS<sub>2</sub> on Si/SiO<sub>2</sub>.

experiences on the Ti<sub>3</sub>C<sub>2</sub> MXene multilayer more closely resembles to the biaxial strain with no selection on the in-plane direction. Lloyd *et al.* demonstrated that the Raman peaks red-shift linearly at a rate of 1.7 cm<sup>-1</sup>/‰ for the A<sub>1g</sub> mode and 5.2 cm<sup>-1</sup>/‰ for the E<sub>2g</sub><sup>1</sup> mode.<sup>31</sup> As the E<sub>2g</sub><sup>1</sup> mode corresponds to an in-plane vibration and the atoms in A<sub>1g</sub> mode vibrate out-of-plane (Fig. 2e), it would be more appropriate to use the E<sub>2g</sub><sup>1</sup> mode to determine the in-plane strain. According to the linear rates, a redshift of 3.3 cm<sup>-1</sup> from the E<sub>2g</sub><sup>1</sup> mode indicates that the local strain is about ~0.6‰, which should simultaneously soften the A<sub>1g</sub> mode by ~1.0 cm<sup>-1</sup>. Nevertheless, the observed redshift in Fig. 3a is 2.9 cm<sup>-1</sup> (>1.0 cm<sup>-1</sup>) for the A<sub>1g</sub> mode. On the other hand, the red-shifted A<sub>1g</sub> mode could be attributed to the electron doping effect which hardly affects the E<sub>2g</sub><sup>1</sup> mode because of symmetry.<sup>32</sup> If the remaining shift of ~1.9 cm<sup>-1</sup> is entirely due to the doping effect, it corresponds to an electron density of 5–6 × 10<sup>12</sup> cm<sup>-2</sup>, which would lead to an increase in the line width by a factor of 1.5.<sup>32</sup> Note that the doped electrons could come from trapped charges at the interface, as discussed in earlier reports.<sup>11,35</sup> We extracted the full width at half maximum and found that while the line widths of the E<sub>2g</sub><sup>1</sup> mode are similar, the A<sub>1g</sub> peak is broadened from 4.4 cm<sup>-1</sup> on Si/SiO<sub>2</sub> to 6.6 cm<sup>-1</sup> on Ti<sub>3</sub>C<sub>2</sub> MXene. The broadened line width is consistent with the electron doping effect.

We further examined the modulation of photoluminescence (PL) response by Ti<sub>3</sub>C<sub>2</sub> MXene. As expected, 1L MoS<sub>2</sub> on Si/SiO<sub>2</sub> exhibits A exciton and B exciton peaks at ~1.85 eV and ~2.02 eV, respectively. The emission from 1L MoS<sub>2</sub> on Ti<sub>3</sub>C<sub>2</sub> MXene is suppressed. Meanwhile, the A excitonic peak is red-shifted by ~50 meV. We first ruled out the effect from Coulomb engineering since the dielectric constant of Ti<sub>3</sub>C<sub>2</sub> MXene<sup>36</sup> is on the same order as that of SiO<sub>2</sub>. According to Lloyd *et al.*, the excitonic peaks in MoS<sub>2</sub> shift linearly at a rate of -99 ± 6 meV/‰.<sup>31</sup> Based on the strain determined from the E<sub>2g</sub><sup>1</sup> mode, we expect a redshift of 59 meV from the A exciton, which is larger than the observed value. Moreover, the electron doping effect would

result in an additional redshift on top of the strain-induced shift.<sup>37</sup> The inconsistency between the shifts of the E<sub>2g</sub><sup>1</sup> mode and the A excitonic complex indicates that one needs to be careful with the determination of strain status, which we will discuss further in the later text.

#### Raman spectra of few-layer MoS<sub>2</sub> on Ti<sub>3</sub>C<sub>2</sub> MXene

We extended our study to few-layer and bulk MoS<sub>2</sub> and plotted the fingerprint peaks in Fig. 4. Similar to 1L MoS<sub>2</sub>, both A<sub>1g</sub> and E<sub>2g</sub><sup>1</sup> modes soften. In addition, the low-frequency interlayer shear (S) mode also red-shifts. Compared to the intralayer in-plane mode (E<sub>2g</sub><sup>1</sup>), a smaller shift is observed in the interlayer in-plane vibration (S mode). In 3L (bulk), the S mode red-shifts by 0.4 (0.5) cm<sup>-1</sup>, while the E<sub>2g</sub><sup>1</sup> mode is down-shifted by 2.0 (1.1) cm<sup>-1</sup>. Our results indicate that while in-plane strain modifies the interatomic distance and shifts the intralayer

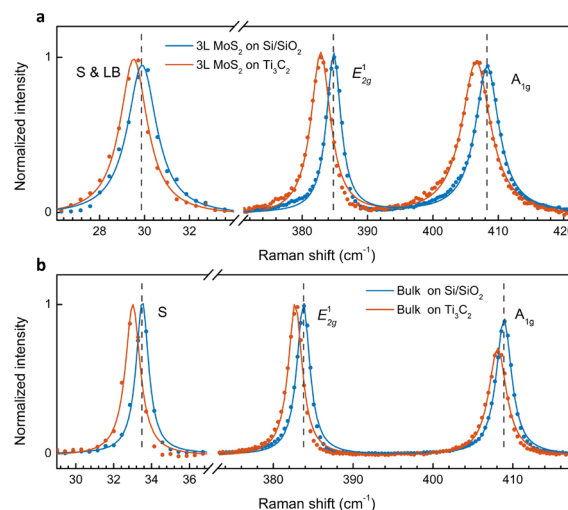


Fig. 4 Raman spectra of 3L (a) and bulk (b) MoS<sub>2</sub> on Ti<sub>3</sub>C<sub>2</sub> MXene in comparison with the counterparts on Si/SiO<sub>2</sub>.



vibrational modes, it has a lower effect on the interlayer vibrations where the whole layers move as a single unit. Our observation is also consistent with an earlier report on strain-dependent low-frequency modes in MoS<sub>2</sub>.<sup>38</sup>

The A<sub>1g</sub> mode in 3L and bulk also red-shifts by a slightly smaller magnitude compared to the E<sub>2g</sub><sup>1</sup> mode (1.7 cm<sup>-1</sup> vs. 2.0 cm<sup>-1</sup> in 3L; 0.8 cm<sup>-1</sup> vs. 1.1 cm<sup>-1</sup> in bulk). Note that the shift rate varies as a function of thickness. Experimentally, Hui *et al.* demonstrated that the shift ratio of E<sub>2g</sub><sup>1</sup> to A<sub>1g</sub> is ~1.5 in 3L under biaxial strain.<sup>39</sup> If we use the E<sub>2g</sub><sup>1</sup> mode to determine the strain value, the strain-induced shift of the A<sub>1g</sub> mode should be 1.3 cm<sup>-1</sup>, smaller than the observed shift of 1.7 cm<sup>-1</sup>. The additional redshift of 0.4 cm<sup>-1</sup> could be attributed to the electron doping effect, similar to the analysis for 1L. Although the line width of the A<sub>1g</sub> peak shows negligible change, different from that in 1L, the doping-induced redshift of 0.4 cm<sup>-1</sup> in 3L is much smaller than that in 1L (1.9 cm<sup>-1</sup>). As a result, the line width is hardly affected due to the smaller doping density. The doping effect in 3L MoS<sub>2</sub> is also confirmed from the PL spectra (Fig. S2†).

### Discussion on the possible laser heating effect

The laser power we used for the above measurements was 0.5 mW, which is not large for MoS<sub>2</sub>. Nonetheless, we conducted excitation power-dependent measurements on another sample with laser power ranging from 0.05 mW to 0.7 mW. As shown in Fig. 5, the E<sub>2g</sub><sup>1</sup> mode exhibits a constant peak position for 1L MoS<sub>2</sub> on Si/SiO<sub>2</sub>, while the maximum redshift from the A<sub>1g</sub> peak is ~0.2 cm<sup>-1</sup>, which is within the resolution of our measurements. This indicates that the laser heating effect is negligible.

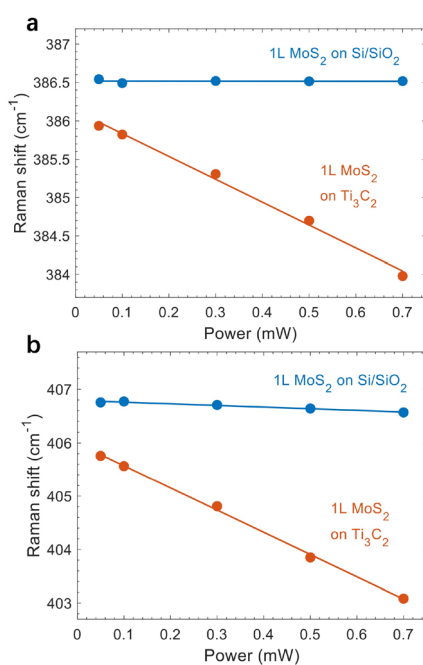


Fig. 5 Raman peak positions as a function of excitation power. (a and b) Peak positions of the E<sub>2g</sub><sup>1</sup> (a) and A<sub>1g</sub> (b) modes. Dots represent experimental data and lines correspond to a linear fitting.

However, it is surprising to see that both peaks red-shift substantially as a function of power for 1L MoS<sub>2</sub> on Ti<sub>3</sub>C<sub>2</sub> MXene. Considering that the thermal conductivity of Ti<sub>3</sub>C<sub>2</sub> MXene is higher than that of SiO<sub>2</sub>,<sup>40,41</sup> heat dissipation should be effective *via* the Ti<sub>3</sub>C<sub>2</sub> MXene layer. Nevertheless, the laser-induced redshifts indicate that the Ti<sub>3</sub>C<sub>2</sub> MXene layer absorbs more heat upon laser illumination, resulting in a smaller temperature gradient and thus less effective heat transfer. We note that the power-induced shifts in both Raman peaks and PL emission are reversible (Fig. S3†), which further supports the heating effect.

As both A<sub>1g</sub> and E<sub>2g</sub><sup>1</sup> modes soften linearly without saturation, the absence of nonlinear effects indicates that the laser-induced shifts are linear below 0.7 mW.<sup>42</sup> Therefore, we used  $\omega(P) = \omega_0 + \chi_p(P)$  to fit the power-dependent peak positions. Here,  $P$  is the excitation power,  $\omega_0$  is the intrinsic peak position without heating effects, and  $\chi_p$  is the power coefficient. For 1L MoS<sub>2</sub> on Ti<sub>3</sub>C<sub>2</sub> MXene, we found that  $\chi_p = -3.0$  cm<sup>-1</sup> and  $\omega_0 = 386.1$  cm<sup>-1</sup> for the E<sub>2g</sub><sup>1</sup> mode, and  $\chi_p = -4.2$  cm<sup>-1</sup> and  $\omega_0 = 406.0$  cm<sup>-1</sup> for the A<sub>1g</sub> mode (Fig. 5, red). The extracted power coefficients are much larger than those from Si/SiO<sub>2</sub>-supported (Fig. 5, blue) and sapphire-supported MoS<sub>2</sub>,<sup>42</sup> but smaller than the values observed for suspended monolayer MoS<sub>2</sub>.<sup>42</sup> After subtracting the heat-induced shift, we still obtained a redshift of 0.4 cm<sup>-1</sup> for the E<sub>2g</sub><sup>1</sup> mode in 1L MoS<sub>2</sub>, which corresponds to 0.08% strain. Such a small in-plane strain causes a negligible shift in the A<sub>1g</sub> mode, which implies that the 0.8 cm<sup>-1</sup> shift (corrected after subtracting the heating effect) for the A<sub>1g</sub> mode is mainly due to the electron doping effect. We note that using the lowest excitation power is not necessarily the best method for measurements since destructive interference from the substrate may lower the Raman intensity and affect the signal-to-noise ratio.<sup>11</sup> Instead, performing a detailed power-dependent measurement in the low and moderate range should be appropriate to subtract the laser heating effect. In addition to 1L MoS<sub>2</sub>, we further conducted power-dependent Raman scattering and PL measurements on 3L MoS<sub>2</sub> (Fig. S4 and S5†), which also corroborate the laser heating effect. Additionally, the temperature-dependent shifts of E<sub>2g</sub><sup>1</sup> and A<sub>1g</sub> modes from 150 K to 300 K are shown in Fig. S6,† where both peaks shift linearly, consistent with the power-dependent measurements.

## Conclusions

In summary, our work demonstrates the substrate effect of Ti<sub>3</sub>C<sub>2</sub> MXene on MoS<sub>2</sub> in Raman spectroscopy. Compared to MoS<sub>2</sub> on Si/SiO<sub>2</sub>, we observed redshifts of the fingerprint peaks from MoS<sub>2</sub> on Ti<sub>3</sub>C<sub>2</sub> MXene and explained these shifts based on the vibrational nature of each peak. The in-plane E<sub>2g</sub><sup>1</sup> mode is more sensitive to strain which arises from both sample fabrication and lattice mismatch, but a small variation in strain hardly shifts the out-of-plane A<sub>1g</sub> mode. We attributed the down-shifted A<sub>1g</sub> mode to the electron doping effect, which is also confirmed by the suppressed and red-shifted PL emission. In addition to the monolayer, we showed that the modulation from Ti<sub>3</sub>C<sub>2</sub> MXene is also present in few-layer and bulk MoS<sub>2</sub>.



Furthermore, we demonstrate that laser excitation power plays a vital role in determining the external perturbations and the magnitude of the heat-induced redshifts varies depending on the underlying substrate. As Raman spectroscopy has been widely used as a nondestructive tool to identify strain and doping effects,<sup>43–45</sup> our results show that a careful power-dependent measurement is essential to subtract the laser-induced shifts and extract the pure modulation from the substrate.

Our work contributes to the understanding of interfacial interaction between  $\text{Ti}_3\text{C}_2$  MXene and  $\text{MoS}_2$  and also provides some insights into the application of  $\text{MoS}_2$ - $\text{Ti}_3\text{C}_2$  heterostructures. While the local heating effect from  $\text{Ti}_3\text{C}_2$  MXene could potentially deteriorate the performance of  $\text{MoS}_2$ - $\text{Ti}_3\text{C}_2$  MXene in nanoelectronics, the  $\text{Ti}_3\text{C}_2$  MXene-induced strain and doping, on the other hand, may improve the performance of  $\text{MoS}_2$  as an electrocatalyst in the hydrogen evolution reaction.<sup>46</sup>

## Methods

### Synthesis of $\text{Ti}_3\text{C}_2$ MXene free-standing paper

A solution of 9 M hydrochloric acid (HCl) and 7.5 M potassium fluoride (KF) was prepared as the etching solution. 4 g of  $\text{Ti}_3\text{AlC}_2$  was added slowly to 80 mL of the solution and stirred at 35 °C for 48 h using magnetic stirring in an oil bath for uniform heating. Subsequently, the solution was washed until the pH level was near neutral. The supernatant was discarded, leaving purified MXene as sediment. DI water was added to it, followed by shaking, and vacuum-filtration.

For delamination, 1 g of  $\text{Ti}_3\text{C}_2$  MXene was added to 35 mL of 5 M LiCl, shaken manually for a minute, and left to soak for 24 h at room temperature. The mixture was centrifuged, and the supernatant was decanted to remove concentrated LiCl. Fresh DI water was added for washing followed by centrifugation and discarding the supernatant. The washing process was repeated three times. After washing, DI water was added, and the mixture was bath sonicated for 1 h followed by centrifugation at 5000 rpm for 1 h. The supernatant was collected and DI water was again added, followed by repeated sonication and centrifugation, until a clear supernatant was obtained. The collected supernatants were combined, shaken and vacuum-filtered to make a free-standing MXene paper. The  $\text{Ti}_3\text{C}_2$  MXene multi-layers were produced by mechanical exfoliation from the MXene paper. The Raman spectrum of  $\text{Ti}_3\text{C}_2$  MXene paper is shown in Fig. S7,<sup>†</sup> and the Energy Dispersive Spectroscopy (EDS) mapping image of the exfoliated flakes is shown in Fig. S8.<sup>†</sup>

### Raman and PL spectroscopy measurements

We carried out the optical measurement by using a home-built setup. The measurements were conducted in a backscattering configuration, excited with a 532 nm laser. The excitation power was kept at 0.5 mW for Fig. 2–4 and varied between 0.05 mW and 0.7 mW for the laser heating effect study (Fig. 5). To reach a low-frequency Raman shift of  $\sim 10\text{ cm}^{-1}$ , we used volume Bragg grating filters (OptiGrate) to block the laser line. The backscattered signal was collected through a 100× objective

and dispersed by an 1800  $\text{g mm}^{-1}$  (Raman) or 300  $\text{g mm}^{-1}$  (PL) grating before being detected by a liquid nitrogen-cooled charge coupled device (Princeton Instruments, PyLoN 1340 × 400 pixels CCD). The spectral resolution of our Raman spectroscopy measurements is  $\sim 0.7\text{ cm}^{-1}$ . Except for the temperature-dependent measurements, all spectra were taken at room temperature.

## Data availability

The data that support the findings of this work are available in the manuscript and its ESI.<sup>†</sup>

## Author contributions

Conceived and designed the experiments: X. L., Q. Z. and M. N. Sample fabrication: E. P., E. L., K. A., A. M., F. W., A. S. and M. B. Data acquisition: E. P., Q. Z. and K. A. Data analysis: X. L., E. P., Q. Z. and M. N. Writing – original draft: X. L., E. P. and Q. Z. Writing – review & editing: X. L., E. P., Q. Z. M.N. and E. L. All authors reviewed the manuscript.

## Conflicts of interest

There are no conflicts to declare.

## Acknowledgements

Acknowledgment is made to the donors of the American Chemical Society Petroleum Research Fund for partial support of this research. X. L. acknowledges support from the Tulane University startup fund. A. M., E. L. and M. N. were supported by the National Science Foundation under Grant No. DMR-2048164.

## References

- 1 B. Anasori and M. Naguib, *MRS Bull.*, 2023, **48**, 238–244.
- 2 M. R. Lukatskaya, O. Mashtalir, C. E. Ren, Y. Dall'Agnese, P. Rozier, P. L. Taberna, M. Naguib, P. Simon, M. W. Barsoum and Y. Gogotsi, *Science*, 2013, **341**, 1502–1505.
- 3 J. Zhang, Y. Zhao, X. Guo, C. Chen, C.-L. Dong, R.-S. Liu, C.-P. Han, Y. Li, Y. Gogotsi and G. Wang, *Nat. Catal.*, 2018, **1**, 985–992.
- 4 Z. Wang, H. Kim and H. N. Alshareef, *Adv. Mater.*, 2018, **30**, 1706656.
- 5 Y. Ma, N. Liu, L. Li, X. Hu, Z. Zou, J. Wang, S. Luo and Y. Gao, *Nat. Commun.*, 2017, **8**, 1207.
- 6 B. Xu, M. Zhu, W. Zhang, X. Zhen, Z. Pei, Q. Xue, C. Zhi and P. Shi, *Adv. Mater.*, 2016, **28**, 3333–3339.
- 7 H. Kim, Z. Wang and H. N. Alshareef, *Nano Energy*, 2019, **60**, 179–197.
- 8 X. Xu, T. Guo, M. K. Hota, H. Kim, D. Zheng, C. Liu, M. N. Hedhili, R. S. Alsaadi, X. Zhang and H. N. Alshareef, *Adv. Mater.*, 2022, **34**, 2107370.



- 9 N. H. Attanayake, S. C. Abeyweera, A. C. Thenuwara, B. Anasori, Y. Gogotsi, Y. Sun and D. R. Strongin, *J. Mater. Chem. A*, 2018, **6**, 16882–16889.
- 10 A. Macknojaia, A. Ayyagari, D. Zambrano, A. Rosenkranz, E. V. Shevchenko and D. Berman, *ACS Nano*, 2023, **17**, 2421–2430.
- 11 M. Buscema, G. A. Steele, H. S. Van Der Zant and A. Castellanos-Gomez, *Nano Res.*, 2014, **7**, 561–571.
- 12 S. Tongay, W. Fan, J. Kang, J. Park, U. Koldemir, J. Suh, D. S. Narang, K. Liu, J. Ji and J. Li, *Nano Lett.*, 2014, **14**, 3185–3190.
- 13 C. H. Lui, Z. Ye, C. Ji, K.-C. Chiu, C.-T. Chou, T. I. Andersen, C. Means-Shively, H. Anderson, J.-M. Wu and T. Kidd, *Phys. Rev. B:Condens. Matter Mater. Phys.*, 2015, **91**, 165403.
- 14 H. Fang, C. Battaglia, C. Carraro, S. Nemsak, B. Ozdol, J. S. Kang, H. A. Bechtel, S. B. Desai, F. Kronast and A. A. Unal, *Proc. Natl. Acad. Sci. U.S.A.*, 2014, **111**, 6198–6202.
- 15 K.-G. Zhou, F. Withers, Y. Cao, S. Hu, G. Yu and C. Casiraghi, *ACS Nano*, 2014, **8**, 9914–9924.
- 16 H. Li, J.-B. Wu, F. Ran, M.-L. Lin, X.-L. Liu, Y. Zhao, X. Lu, Q. Xiong, J. Zhang and W. Huang, *ACS Nano*, 2017, **11**, 11714–11723.
- 17 A. Castellanos-Gomez, M. Buscema, R. Molenaar, V. Singh, L. Janssen, H. S. Van Der Zant and G. A. Steele, *2D Mater.*, 2014, **1**, 011002.
- 18 F. Pizzocchero, L. Gammelgaard, B. S. Jessen, J. M. Caridad, L. Wang, J. Hone, P. Bøggild and T. J. Booth, *Nat. Commun.*, 2016, **7**, 11894.
- 19 H. Zhang, Y. Ma, Y. Wan, X. Rong, Z. Xie, W. Wang and L. Dai, *Sci. Rep.*, 2015, **5**, 8440.
- 20 X. Lu, M. I. B. Utama, J. Zhang, Y. Zhao and Q. Xiong, *Nanoscale*, 2013, **5**, 8904–8908.
- 21 C. Lee, H. Yan, L. E. Brus, T. F. Heinz, J. Hone and S. Ryu, *ACS Nano*, 2010, **4**, 2695–2700.
- 22 X. Luo, Y. Zhao, J. Zhang, Q. Xiong and S. Y. Quek, *Phys. Rev. B:Condens. Matter Mater. Phys.*, 2013, **88**, 075320.
- 23 Q.-H. Tan, X. Zhang, X.-D. Luo, J. Zhang and P.-H. Tan, *J. Semicond.*, 2017, **38**, 031006.
- 24 T. Wieting and J. Verble, *Phys. Rev. B:Condens. Matter Mater. Phys.*, 1972, **5**, 1473.
- 25 P. N. Ghosh and C. Maiti, *Phys. Rev. B:Condens. Matter Mater. Phys.*, 1983, **28**, 2237.
- 26 Y. Lin, X. Ling, L. Yu, S. Huang, A. L. Hsu, Y.-H. Lee, J. Kong, M. S. Dresselhaus and T. Palacios, *Nano Lett.*, 2014, **14**, 5569–5576.
- 27 X. Lu, X. Luo, J. Zhang, S. Y. Quek and Q. Xiong, *Nano Res.*, 2016, **9**, 3559–3597.
- 28 X. Zhang, X.-F. Qiao, W. Shi, J.-B. Wu, D.-S. Jiang and P.-H. Tan, *Chem. Soc. Rev.*, 2015, **44**, 2757–2785.
- 29 X. Zhang, Q.-H. Tan, J.-B. Wu, W. Shi and P.-H. Tan, *Nanoscale*, 2016, **8**, 6435–6450.
- 30 H. J. Conley, B. Wang, J. I. Ziegler, R. F. Haglund Jr, S. T. Pantelides and K. I. Bolotin, *Nano Lett.*, 2013, **13**, 3626–3630.
- 31 D. Lloyd, X. Liu, J. W. Christopher, L. Cantley, A. Wadehra, B. L. Kim, B. B. Goldberg, A. K. Swan and J. S. Bunch, *Nano Lett.*, 2016, **16**, 5836–5841.
- 32 B. Chakraborty, A. Bera, D. Muthu, S. Bhowmick, U. V. Waghmare and A. Sood, *Phys. Rev. B:Condens. Matter Mater. Phys.*, 2012, **85**, 161403.
- 33 X. Lu, M. I. B. Utama, X. Wang, W. Xu, W. Zhao, M. H. S. Owen and Q. Xiong, *Small*, 2017, **13**, 1701039.
- 34 J.-U. Lee, J. Park, Y.-W. Son and H. Cheong, *Nanoscale*, 2015, **7**, 3229–3236.
- 35 Y. Li, Z. Qi, M. Liu, Y. Wang, X. Cheng, G. Zhang and L. Sheng, *Nanoscale*, 2014, **6**, 15248–15254.
- 36 G. Berdiyrov, *AIP Adv.*, 2016, **6**, 055105.
- 37 K. F. Mak, K. He, C. Lee, G. H. Lee, J. Hone, T. F. Heinz and J. Shan, *Nat. Mater.*, 2013, **12**, 207–211.
- 38 J.-U. Lee, S. Woo, J. Park, H. C. Park, Y.-W. Son and H. Cheong, *Nat. Commun.*, 2017, **8**, 1370.
- 39 Y. Y. Hui, X. Liu, W. Jie, N. Y. Chan, J. Hao, Y.-T. Hsu, L.-J. Li, W. Guo and S. P. Lau, *ACS Nano*, 2013, **7**, 7126–7131.
- 40 S. Callard, G. Tallarida, A. Borghesi and L. Zanotti, *J. Non-Cryst. Solids*, 1999, **245**, 203–209.
- 41 P. Yasaei, Z. Hemmat, C. J. Foss, S. J. Li, L. Hong, A. Behranginia, L. Majidi, R. F. Klie, M. W. Barsoum and Z. Aksamija, *Adv. Mater.*, 2018, **30**, 1801629.
- 42 R. Yan, J. R. Simpson, S. Bertolazzi, J. Brivio, M. Watson, X. Wu, A. Kis, T. Luo, A. R. Hight Walker and H. G. Xing, *ACS Nano*, 2014, **8**, 986–993.
- 43 M. Velicky, A. Rodriguez, M. Bousa, A. V. Krayev, M. Vondracek, J. Honolka, M. Ahmadi, G. E. Donnelly, F. Huang and H. D. Abruna, *J. Phys. Chem. Lett.*, 2020, **11**, 6112–6118.
- 44 M. O'Brien, N. Scheuschner, J. Maultzsch, G. S. Duesberg and N. McEvoy, *Phys. Status Solidi B*, 2017, **254**, 1700218.
- 45 Y. Wang, J. Balgley, E. Gerber, M. Gray, N. Kumar, X. Lu, J.-Q. Yan, A. Fereidouni, R. Basnet and S. J. Yun, *Nano Lett.*, 2020, **20**, 8446–8452.
- 46 S. Bolar, S. Shit, N. C. Murmu, P. Samanta and T. Kuila, *ACS Appl. Mater. Interfaces*, 2021, **13**, 765–780.

